Ultrasonic Analytic-Signal Responses From Polymer-Matrix Composite Laminates

Robert A. Smith[ORCID], Luke J. Nelson, Martin J. Mienczakowski, and Paul D. Wilcox

Abstract—**Ultrasound has been used to inspect composite laminates since their invention but only recently has the response from the internal plies themselves been considered of interest. This paper uses modeling techniques to make sense of the fluctuating and interfering reflections from the resin layers between plies, providing clues to the underlying inhomogeneities in the structure. It shows how the analytic signal, analyzed in terms of instantaneous amplitude, phase, and frequency, allows 3-D characterization of the microstructure. It is found that, under certain conditions, the phase becomes locked to the interfaces between plies and that the first and last plies have characteristically different instantaneous frequencies. This allows the thin resin layers between plies to be tracked through various features and anomalies found in real composite components (ply drops, tape gaps, tape overlaps, and out-of-plane wrinkles), giving crucial information about conformance to design of as-manufactured components. Other types of defects such as delaminations are also considered. Supporting evidence is provided from experimental ultrasonic data acquired from real composite specimens and compared with X-ray computed tomography images and microsections.**

Index Terms—**Analytical models, composite materials, material and defect characterization, phase measurement, signal and image processing, ultrasonic imaging, wave propagation.**

I. INTRODUCTION

IN THE composites manufacturing environment, the nondestructive testing (NDT) profession is increasingly criticized for being unable to provide sufficient information about the defects it detects and the conformance of as-manufactured components to the design [1], [2]. A consequential reduction in confidence that the component will perform adequately leads to risk mitigation in terms of increased thickness of the design and a reluctance to concede defects, thus increasing weight, numbers of repairs, and scrappage rates. Examples of the desirable additional NDT information are: 3-D maps of fiber volume fraction, porosity, out-of-plane ply wrinkling, in-plane fiber waviness, ply-drop and ply-overlap locations, and ply stacking sequence [3].

The body of research aimed at extracting these material characteristics from NDT outputs is evidence for its current importance. Methods have been applied to various NDT modalities such as: X-ray computed tomography (X-ray CT) [4]–[7], terahertz imaging [8], [9], eddy currents [10], [11], ultrasonic guided waves [12], near infrared [13], optical [14]–[17], and ultrasound [18]–[21]. Many of these methods are limited to specific material characteristics or are difficult to deploy due to sample-size limitations or data acquisition constraints. Manufacturers are reluctant to deploy additional NDT methods and, of the above methods, only pulse-echo ultrasonic inspection is already routinely used in industrial settings to detect inclusions, delaminations, and porosity in carbon-fiber reinforced plastic (CFRP) components. Extending its use to detect other features (ply wrinkling, fiber orientation, etc.) is, therefore strongly desirable, but has been limited due to the lack of understanding of the interaction of ultrasound with the internal plies and fiber-tows that is required to image such features reliably.

The information about the composite that would increase confidence in its fitness for purpose is at the scale of a ply or a fiber tow in the laminate; individual fibers do not have to be tracked and no defects smaller than 0.1 mm in size have been shown to be significant. Plies are commonly 0.125, 0.189, or 0.250 mm in thickness. Fiber tows—bundles of fibers from which preimpregnated (pre-preg) plies are formed—can contain from 1000 to 12 000 fibers of diameter approximately 0.007 mm, making fiber tows within a ply between 0.5- and 6-mm wide. Thus, the range of ultrasonic wavelengths (0.2–2 mm) and manageable focal beamwidths (0.5–3 mm) commonly used for ultrasonic NDT should be capable of resolving any irregularities on the required scale. It is not due to insufficient resolution that the desired ultrasonic NDT capabilities have not been forthcoming for composite materials. The shortcomings of NDT are, instead, explained by a lack of inversion methods for linking the ultrasonic response to the microscopic variations in the material, due to a lack of understanding of the ultrasonic interaction with composite plies, fiber tows, and defects. Increased computational power, coupled with recent advances in ultrasonic modeling methods [22]–[25], has enabled this paper, which provides a deeper understanding of the ultrasonic interaction with composite laminates.

This paper builds on previous empirical attempts to extract ply-specific information such as in-plane fiber-tow orientation to determine ply stacking sequence [26]–[28], out-of-plane ply wrinkling, and in-plane fiber-waviness mapping [28]–[30]. This previous work used either the "RF" ultrasonic waveform

or its envelope. Whilst this is adequate for measuring misaligned plies through wrinkles, it is unreliable for tracking ply drops and overlaps because amplitude variations can be caused by many other phenomena such as porosity and layer-thickness changes, so a different method is required. Pain and Drinkwater [31], [32] and Li *et al.* [33] have shown the potential for using the instantaneous phase to track plies in composites, which was developed further by Smith *et al.* [34]. Zardan *et al.* [20] detected and identified out-of-plane ply waviness by considering the deviation of the ultrasonic beam through resin wedges. However, they have yet to propose an inversion method to map the ply locations and quantify the angular deviations.

The aim of this paper is to demonstrate that characteristic signatures from microstructural variations that exist in the reflected analytic signals from composite laminates and that an automated process can be used for mapping these variations.

Following a background section in which the analytic signal, ultrasonic model, and previous modeling predictions are described with reference to published literature, the novel modeling predictions of characteristic signatures are shown. This paper uses a 1-D analytical model, which shows that instantaneous phase, amplitude, and frequency can be used to distinguish between various changes in the laminate and to track and map those variations. The analytic-signal response is studied for several different defect types including ply drops, delaminations, tape gaps and overlaps, and out-of-plane ply wrinkling. Finally, the resulting analysis method is demonstrated on real specimens and compared with microsections and X-ray Micro-CT scans.

II. Background

A. Ultrasonic Model

An ultrasonic model has been implemented in MATLAB and used to simulate the pulse-echo response of a composite laminate. It is one of a number of ways of obtaining the exact solution to a 1-D wave-propagation problem and is based on the recursive analytical multilayer model developed in [22], which had been benchmarked against various other models and experiment; it is described more fully in [34]. The Hashin mixture rules for long-fiber composites [35] are applied to determine effective-medium properties for the composite plies based on a fiber volume fraction which is allowed to vary to compensate for ply-thickness variations, such as in wrinkled regions. The transverse compression modulus is used for ultrasonic propagation across plies, for which case the isotropic-fiber expressions of Hashin [35] still apply—as shown by Hashin [36]. Interply layers are modeled as pure resin. The model calculates the frequency-dependent response of a laminate and includes attenuation due to visco-elastic damping in the interply resin layers and the resin phase of the composite plies. In this paper, two scenarios are used for embedding the composite laminate either: 1) in water as for immersion scanning or 2) in a matched homogeneous, isotropic medium with the same effective-medium bulk properties as a carbon fiber composite with a 60% fiber volume fraction, to view the ply responses without any interference from the front and back surfaces.

A plane-wave input-pulse is simulated using a Gaussian-weighted spectrum with a constant phase, ϕ_0 at all frequencies, making ϕ_0 the phase at the time of the peak in the envelope. This input pulse accounts for both the transmission and reception responses of the transducer. It is applied by multiplication in the frequency domain prior to the use of an inverse Fourier transform to determine a realistic time-domain analytic-signal response of the laminate. Zero time is at the time-of-flight for the front-surface reflection. No artificial noise was added for the simulations presented here.

In order to investigate how the normal-incidence reflected response varies over a structural feature such as a ply drop, wrinkle, or delamination, the 1-D model has been applied for the set of layer thicknesses and properties under each point on the surface of the structure and a pseudo B-scan image is built up from the adjacent waveform responses. Whilst this is an over-simplification for laminates with very local variations, it is a reasonable assumption for most nonwoven composites when inspected with focal beamwidths of 2 mm or less, as used in this paper. An investigation of more local effects will be the subject of a future project and publication.

B. Analytic Signal

The analytic signal was defined by Gabor [37] in 1946. Gammell [38] demonstrated that it is "the optimal estimator of interface location for echo signals of the type commonly used in ultrasound analysis." As such, it is a useful formulation for interpreting the ultrasonic response from composite laminates and locating the echoes from the various layers. It is a complex function describing the time dependence of the acoustic signal received at a pulse-echo transducer and comprises a measurable (real) component and an imaginary component in quadrature phase with it. As shown by Heyser [39], the analytic signal accurately describes the energy rate-of-arrival whilst the real part is unable to do this alone. During each cycle, the energy transfers between the real and imaginary components like it does between particle velocity (kinetic energy) and particle displacement (potential energy) in an acoustic wave. The mathematical form used in this paper is

$$x_a(t) = A(t)e^{i\phi(t)} \tag{1}$$

where $A(t)$ is the instantaneous amplitude and $\phi(t)$ is the instantaneous phase at time t. The imaginary part of the analytic signal is calculated by applying a Hilbert transform to the measured (real) waveform [40]. The instantaneous frequency, $f(t)$, is the rate of change of phase at time t in the response at the measurement location and is given [41] by

$$f(t) = \frac{1}{2\pi}\frac{d\phi}{dt}. \tag{2}$$

The instantaneous amplitude, $A(t)$, is the magnitude, or envelope, of the signal [42].

C. Previous Modeling Predictions

The simulated analytic signal shown in Fig. 1 corresponds to the ultrasonic response of an 8-ply composite embedded in a matching infinite homogenous medium. In the context of
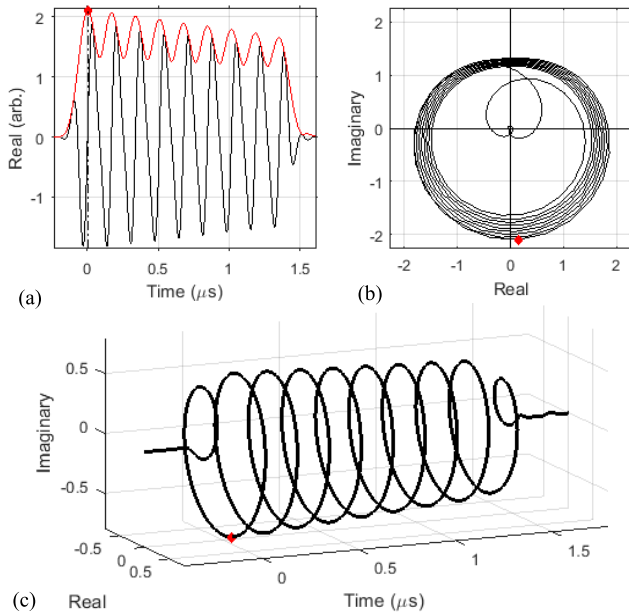
Fig. 1. Simulated pulse-echo response from eight 0.24-mm-thick composite plies separated by 0.01-mm-thick resin layers with matched entry/exit media. The incident pulse spectrum has a center frequency at the fundamental ply resonance of 6 MHz, a 6-MHz bandwidth, and a phase ϕ_0 of zero. (a) RF (real) signal (black) and instantaneous amplitude (red). (b) and (c) Complex analytic signal. The red diamond symbols are at the points of maximum instantaneous amplitude, corresponding to zero time-of-flight.

this result, the predictions previously proposed in [34] can be summarized as follows.

1) Internal reflections occur primarily at the resin-rich layers between plies, giving rise to a weak resonant behavior and peaks in the instantaneous amplitude as shown by the red line in Fig. 1(a).

2) At the fundamental ply resonance frequency, one wavelength is equal to the round-trip path length through a ply; the instantaneous phase traverses approximately 2π radians for each ply in the laminate as seen in Fig. 1(b) where each turn of the helix about the time axis corresponds to 2π radians change of instantaneous phase.

3) The instantaneous phase at the time of the reflection from a resin layer appears to be close to $\phi_0 - \pi/2$ radians, shown as red dots in Fig. 1(b), where ϕ_0 is the instantaneous phase at the peak instantaneous amplitude of the input pulse and is zero for Fig. 1.

4) The phase tracks the location of resin layers well when center frequency and pulse-echo bandwidth are both at approximately the fundamental ply resonance frequency.

5) A narrower bandwidth allows too little variation in resonance frequency to track varying thickness plies because the input-pulse center frequency dominates over the ply resonance.

6) A wider bandwidth allows the second resonance of a ply (termed the second harmonic) to be excited to a sufficient amplitude for a phase change of 4π radians to be observed for a thicker ply, implying a double ply instead of a thicker single ply.

This paper explores the validity of the above predictions quantitatively and proposes using the instantaneous frequency $f(t)$, (2) to improve the distinction between different microstructural features, defect types, and causes of ultrasonic-response variations. A simple example is that a significant second-harmonic amplitude in the response, due to a thick ply, would be clearly visible as a doubling of the instantaneous frequency and would be distinguishable from two thin plies because the instantaneous amplitude is lower in the middle of a ply than at a resin layer.

III. MODELING PREDICTIONS

A. Ply Interactions

All modeling in this paper uses a nominal ply spacing (one ply thickness plus one resin-layer thickness) of 0.25 mm, which has a fundamental resonance frequency of approximately 6 MHz such that a single cycle fits in the time of a round-trip through a ply and back. The resulting predictions can be applied to other ply spacings by simple scaling using the methods described below. Fig. 2(a) shows the frequency response (frequency-dependent reflection coefficient) of a single ply between two resin layers, all embedded in matching entry/exit media. This is the product of the single-ply response (a "half-wave resonator" with maxima at integer multiples of the half-wave resonance frequency, including a peak at zero frequency) and the 0.01 mm resin-layer response (a "quarter-wave resonator," which is zero at zero frequency and rises monotonically to its first maximum at 72 MHz) [22]. Over the frequency range from 0 to 15 MHz, the overall response exhibits maxima at 6 MHz, termed here the fundamental resonance, and 12 MHz, termed the second harmonic. These correspond to the half- and full-wave resonances of the ply, respectively. There is also a maximum at approximately 1.5 MHz, termed the subharmonic, which is merely a result of the above multiplication of two responses and only exists locally for each ply because it destructively interferes with reflections from adjacent plies.

The nth harmonic frequency for other ply spacings can be calculated by a simple scaling of frequency

$$f_n = \frac{nc}{2l} \tag{3}$$

where f_n is the frequency of the nth harmonic resonance, c is the sound velocity in the composite ply, and l is the ply spacing. n takes the value 1 for the fundamental resonance and 2 for the second harmonic.

The three resonance peaks shown in Fig. 2(a) effectively define three resonance modes in the pulse-echo response of a single ply, the dominant mode depending on the input-pulse characteristics and the ply thickness. These modes need to be understood for optimized characterization of composites. Fig. 2(b) illustrates how the dominant mode (black dot) varies with ply thickness using the simulated amplitude response of a single ply between two resin layers with matched entry/exit media. The modes can be described as follows, with reference to (3) and Fig. 2(b), where f_c is the input-pulse center frequency, f_1 is the fundamental resonance frequency ($n = 1$) for the ply:
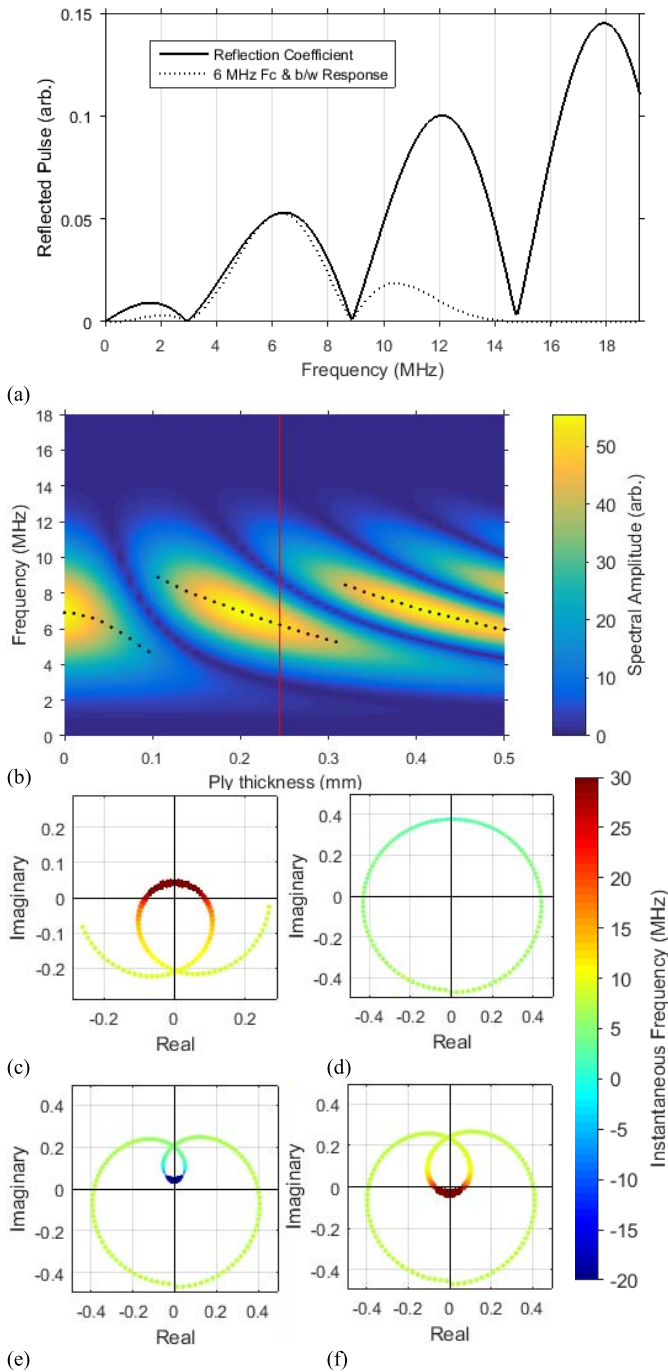
Fig. 2. Simulated ultrasonic response of a single (60% fiber volume fraction) ply between 0.01-mm-thick resin layers and matched entry/exit media, showing subharmonic, fundamental, and second-harmonic resonances [22]. (a) 0.24-mm ply reflection-coefficient spectrum (solid line) and reflected spectrum using a 6-MHz center frequency and 6-MHz bandwidth input pulse (dotted line). The latter is also at the red line in (b), showing influence of ply thickness, for each of which, black dots highlight the dominant resonance frequency: the subharmonic mode for ply thickness less than 0.1 mm, fundamental mode between 0.1 and 0.32 mm, and second-harmonic mode above 0.32 mm. (c)–(f) Analytic-signal plots with color giving instantaneous frequency for ply thicknesses of: (c) 0.10 mm, (d) 0.24 mm, (e) 0.30 mm, and (f) 0.32 mm (second-harmonic mode).

1) the subharmonic mode ($n = (1/4)$): $f_c/f_1 \leq 0.4$;
2) the fundamental-resonance mode ($n = 1$):
    $0.4 < f_c/f_1 < 1.3$; one cycle is reflected per ply;
3) the second-harmonic mode ($n = 2$): $f_c/f_1 \geq 1.3$; two cycles are reflected per ply.

Fig. 2(c)–(f) illustrates the analytic-signal response for a single ply between resin layers with matching entry/exit media, so starting and ending with a phase of $\phi_0 - \pi/2$ radians. The instantaneous frequency is shown as the color of the dots, spaced in time at the sample rate where green is approximately the input-pulse center frequency of 6 MHz, red is an increase and blue a decrease. Fig. 2(d) shows the fundamental resonance mode—the center frequency is near the nominal ply resonance. The instantaneous frequency increases as the ply becomes thinner in Fig. 2(c) and decreases as it gets thicker, eventually forming an additional loop opposite the resin-layer phase, corresponding to the middle of a ply as in Fig. 2(e). This loop accommodates the same phase progression within a longer time period. At this stage, the instantaneous frequency is negative and the amplitude is very low as the analytic signal approaches the origin. If the ply thickens further, the loop suddenly goes beyond and encloses the origin in Fig. 2(f), adding 2π to the phase progression in the ply and indicating the dominance of the second-harmonic mode. This is a significant discovery as such sudden changes in instantaneous frequency are observed experimentally in the middle of plies.

The three components of the analytic-signal response are illustrated in Fig. 3 for 8 plies of thickness 0.24 mm and resin layers of 0.01-mm thickness, immersed in water. Instantaneous amplitude and frequency both increase at each resin-layer echo and decrease in the middle of each ply, as in Fig. 2(d) where amplitude is the radius from the origin and frequency is represented by changes in the color and spacing of the dots as they progress from the resin-layer echo at $\phi_0 - \pi/2$ to the mid-ply region at $\phi_0 + \pi/2$.

The prediction that either a particular instantaneous phase or an amplitude peak will be locked to the resin-layer interfaces is considered quantitatively in Fig. 4 as a function of depth in the laminate and thickness of the resin layers. Fig. 4(a) clearly shows that phase is more stable than amplitude for tracking plies, especially where amplitude is affected by the strong surface signal. As the reflection coefficient of a resin layer is approximately proportional to its thickness, this explains the breakdown in phase tracking for very thin resin layers. But, in general, resin-layer thicknesses only vary between 5% and 15% of the ply spacing. For this range, Fig. 4(b) shows there is an underestimate in resin-layer phase-tracking of approximately 15% of the resin-layer thickness (e.g., slope of the thick solid line), combined with a systematic error of less than ±1.5% of the ply spacing. The resolution of the ply tracking is limited by the time resolution of the phase data set; this result was obtained with a time resolution of 0.4 ns, giving a ply-tracking resolution of 0.24% of the ply spacing. In this case, a digitization sample rate of 2.5 GS/s was used, although a lower rate could be used in practice, with interpolation of the phase data to achieve the required resolution. The input-pulse center frequency and bandwidth were equal to the fundamental ply resonance.

The deviations from perfect ply tracking in the absence of noise, shown in Fig. 4, can be explained in terms of two competing influences on the phase of the response. In the absence of interfaces, the phase progression (instantaneous
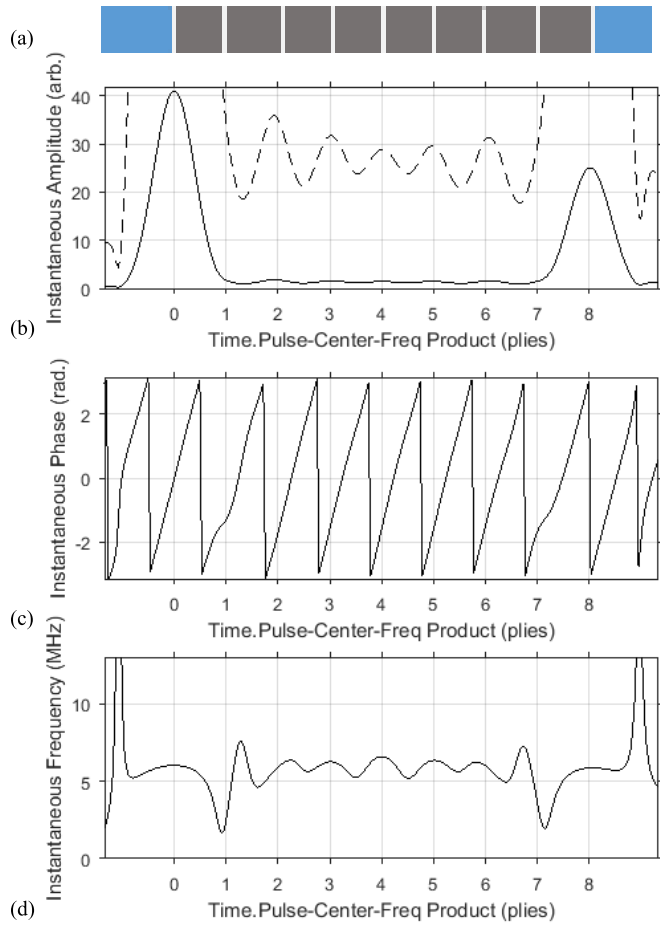
(a)

(b)

(c)

(d)

Fig. 3. Analysis of the simulated response to an input signal with center frequency and bandwidth at the fundamental ply resonance of 6 MHz and an input-signal phase, $\phi_0 = 0$, of (a) eight 0.24-mm-thick plies with 0.01-mm-thick resin layers, embedded in water, (b) instantaneous amplitude with a gain of 1 (solid curve) and 20 (dashed curve), (c) wrapped instantaneous phase, and (d) instantaneous frequency. Note that the phase at the front-surface peak in amplitude (0 on horizontal axis) is zero for an input-pulse phase (ϕ_0) of zero, whilst the phase at the back-surface peak (ply 8) is at $-\pi$ radians (i.e., $\phi_0 - \pi$).
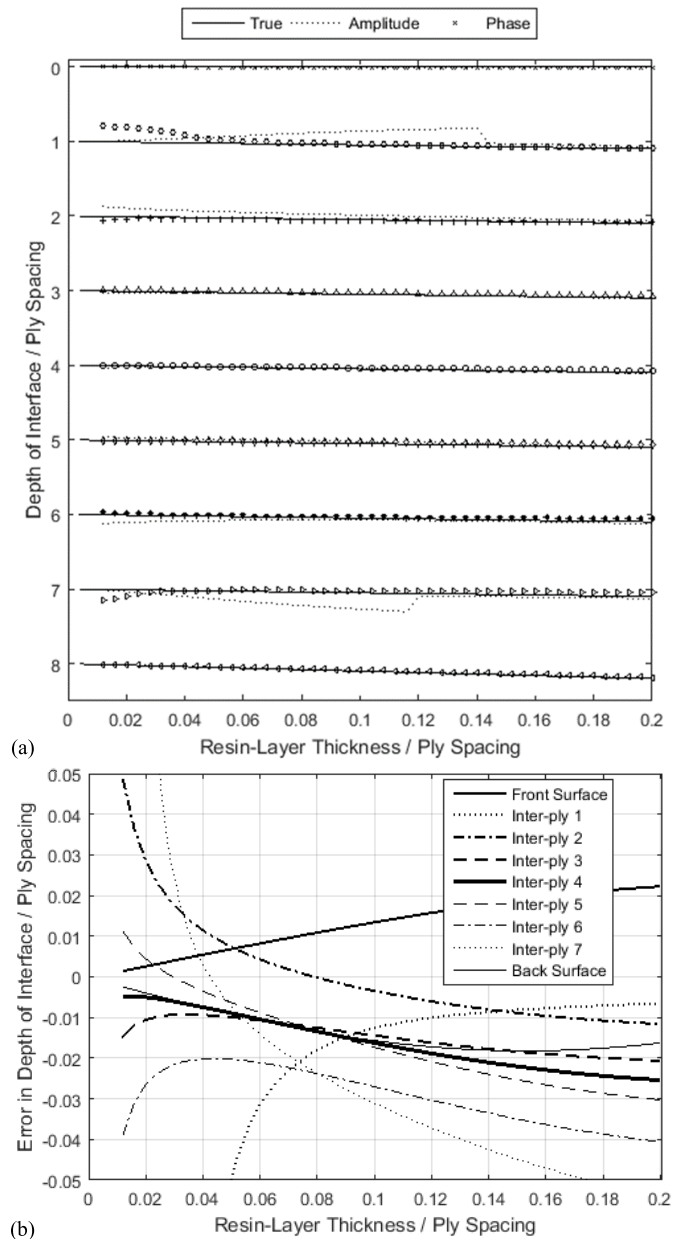

(a)

(b)

Fig. 4. Quantitative assessment of resin-layer interface tracking in a simulated 8-ply laminate in water, with varying resin-layer thickness but no added noise. (a) Comparison of actual center-line (solid line) with instantaneous-amplitude (dotted line) and phase (symbols) location of interfaces. (b) Error in phase tracking: Deviation of measured from actual interface location.

frequency) at a particular depth would be solely dictated by the spectrum of the ultrasound incident at that depth, whilst the resonance frequency of the resin-layer interfaces increases in influence with resin-layer thickness. As the resonance- frequency amplitude is gradually more attenuated with depth and with greater resin-layer thickness, this will also affect the trade-off between these two influences on phase.

B. Front-Surface Echo in Water

In the authors' previous work, the echo from the water-to-composite (front-surface) interface was considered to provide little useful information [34], but it can actually define:
1) the exact time-of-flight to the front surface, set as $t = 0$;
2) the input-pulse instantaneous phase ϕ_0 [at $t = 0$ in Fig. 3(c)].

Simulated responses have shown that the front-surface echo from a composite laminate with a thin surface resin layer is very similar in the time domain to the echo from a

frequency-independent reflector such as a single interface. This implies a close similarity of center frequency, phase, and pulse-echo bandwidth to the input pulse. Therefore, the phase at the peak amplitude of the front-surface echo is a useful estimate of ϕ_0. Simulation has shown this to be within ± 0.1 radians of the actual ϕ_0 for surface resin-layer thicknesses up to 10% of a wavelength and for a center frequency and bandwidth close to the ply resonance.

Given that the wrapped phase at the peak of the reflection from the resin layer between plies 1 and 2 is at $\phi_0 - \pi/2$ radians (predicted in Section III-A), it follows that the
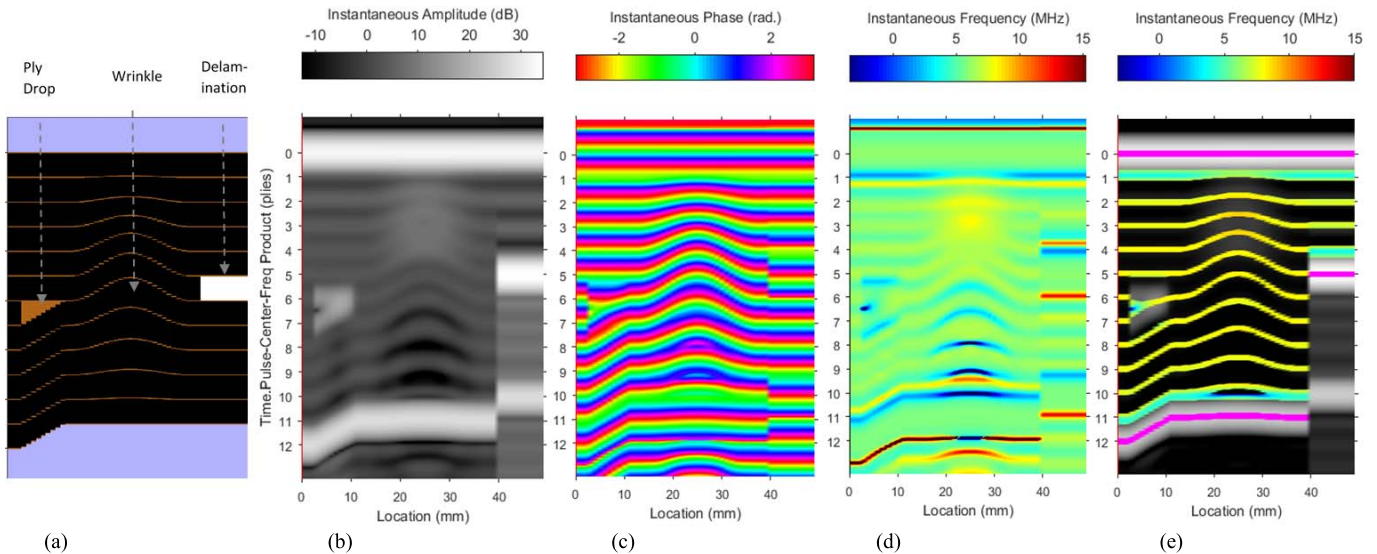
Fig. 5. 12-ply simulation with a ply drop, a wrinkle of amplitude 0.25 mm, and a delamination modeled for ultrasonic propagation as a series of plane-wave 1-D models. Plies of 0.25-mm spacing, 0.1-mm resin layers, and an input pulse with 6-MHz center frequency and bandwidth, and $\phi_0 = 0°$ was used. (a) Schematic of the structure. (b) Instantaneous amplitude. (c) Instantaneous phase. (d) Instantaneous frequency where the fundamental ply resonance is green. (e) Instantaneous amplitude in grayscale with superimposed magenta lines for front-surface, back-surface, and delamination reflections, based on characteristic signatures outlined in the text, whilst other colours, plotted at $\pm\pi/4$ radians around the resin-layer phase, represent instantaneous frequency.

instantaneous phase only increases by $3\pi/2$ radians in the first ply, implying a significantly lower instantaneous frequency following the front-surface echo than between deeper resin layers (as illustrated in Fig. 3(d).

C. Back-Surface Echo

At the back surface of the laminate, the resin-to-water boundary again dominates over the composite-to-resin boundary. In the case of water, or any low-impedance medium, beyond the back surface, the reflection coefficient for acoustic pressure will be negative, resulting in an instantaneous phase at the peak of the reflection of $\phi_0 - \pi$ radians, as seen in Fig. 3(c). As with the front-surface echo, if the phase at the peak of the reflection from the last resin layer (between the last two plies) is at $\phi_0 - \pi/2$ radians, it follows that the instantaneous phase again only increases by $3\pi/2$ radians in the last ply. This has proved to be a useful classifier for the back-surface echo as phase and amplitude are insufficient to distinguish it from an unusually thick resin layer.

IV. CHARACTERISTIC SIGNATURES IN COMPOSITE

For the purposes of investigating characteristic signatures, the ultrasonic plane-wave propagation has been modeled in a series of independent 1-D analytical models with parallel planar interfaces, producing a sequence of waveforms combined as B-scan cross-sectional slices. The structure modeled in Fig. 5 contains a ply drop (on the left) where ply 7 stops and resin fills the gap until adjacent plies join, a wrinkle of amplitude equal to a ply thickness (middle), and a delamination between plies 5 and 6 (right), modeled as 100% porosity in ply 6. Color palettes are chosen deliberately, throughout the paper, as follows. Grayscale is used for amplitude so additional results can be superimposed in color. The *Hue*
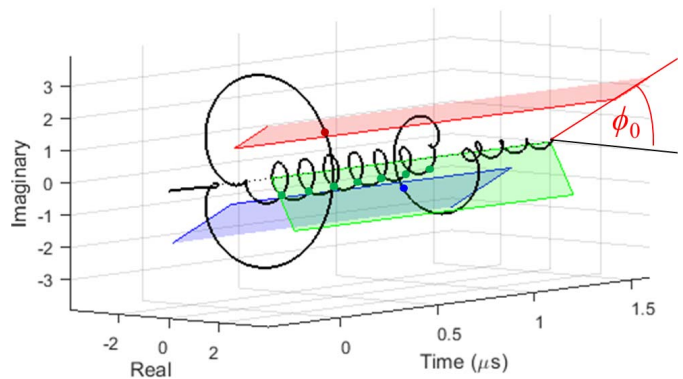

Fig. 6. Illustration of the "analytic-signal gates" on the response from an 8-ply laminate in immersion with an input pulse of phase $\phi_0 = \pi/6$ radians. For interface-classification: red for front-surface (ϕ_0), blue for back surface ($\phi_0 - \pi$), and green for resin layers ($\phi_0 - \pi/2$). Colored dots show gate trigger points.

axis of the "HSV" (hue, saturation, value) color space is used for phase because it uses a cylindrical geometry where angle represents *Hue*, so it wraps in the same way as phase angle [43]. The "Jet" palette is used for frequency to show the fundamental resonance frequency as central green, with increases as yellow–red and decreases as cyan–blue [44].

A. Classification of Interfaces

Fig. 6 illustrates the classification of interfaces using analytic-signal "gates" on a simulated response from an 8-ply laminate in immersion; a gate is a defined surface in complex space through which the analytic signal may pass, marking the time when the gate was "triggered." The front-surface gate (red), at the input-pulse phase ϕ_0 ($\phi_0 = \pi/6$ radians in this case), begins at the start of the waveform with a

minimum instantaneous-amplitude threshold at a user-prescribed percentage of the predetermined maximum in each waveform. When the analytic signal passes through this gate (red dot in Fig. 6), it triggers that time as the time-of-flight of the front-surface echo. After the amplitude has subsided below another prescribed proportion of the front-surface maximum, the back-surface (blue) and resin-layer (green) gates start, with phases of $\phi_0 - \pi$ radians and $\phi_0 - \pi/2$ radians, respectively. Trigger events in the green gate (green dots in Fig. 6) indicate the times-of-flight of the middle of the resin layers. This happens once per cycle of the analytic signal until the back-surface (blue) gate's amplitude threshold (at a predetermined percentage of the front-surface signal) is surpassed (blue dot in Fig. 6) and there has also been a characteristic reduced instantaneous frequency in the previous ply, indicating the time-of-flight of the back surface.

In Fig. 5(e), resin-layer locations are superimposed on amplitude data at all points with phase within $\pm\pi/4$ radians of the resin-layer gate's phase by plotting a color representing instantaneous frequency there, whilst front and back surfaces are shown as magenta lines.

B. Delaminations

The reflection at a delamination, assuming it has a volume of air within it, is similar to the water-backed back-surface echo in all but its larger amplitude [Fig. 5(b)]. As a reduced instantaneous frequency exists in the ply before a delamination, it will be detected as if it is a back-surface echo. Fig. 5(d) shows a characteristic instantaneous frequency rise and fall before the delamination and Fig. 5(e) has it marked as a magenta line on the right, also showing the larger amplitude echo from a delamination than the back surface, and even larger than the front-surface echo. A potential application for this is in automated 3-D mapping of impact damage and generation of 3-D finite-element analysis models [45], [46].

C. Resin-Filled Ply Drops, Tape Gaps, and Overlaps

Tape gaps and overlaps are effectively two ply drops in close proximity and opposite orientation. Therefore, it is sufficient to consider them all as resin-filled ply drops, as modeled by Smith *et al.* [34]. For the ply drop in Fig. 5(b) at location 3–10 mm and a time of approximately 1.1 μs, the instantaneous amplitude is higher at the front and back of the resin wedge than at a normal resin layer. This is because the reflection coefficient of a single composite-to-resin interface is much greater than for a thin resin layer. The model predicts that the peak amplitude is when the resin wedge is 0.2 wavelengths (in resin) thick - 0.1 mm in this case for an input pulse with bandwidth equal to its center frequency. Up to this point, the phase at the peak of the signal reflected from the resin wedge is $\phi_0 - \pi/2$ radians, as normal [see Fig. 7(a)]. But, for the thicker part of the resin wedge—between 0.2 and 0.5 wavelengths thickness—the front and back echoes separate out; the phase at the peak from the front of the resin wedge is $\phi_0 - \pi$ radians and from the back it is ϕ_0, as shown in Figs. 5(c) and 7(c). This causes just a $3\pi/2$ radians phase progression in the plies before and after
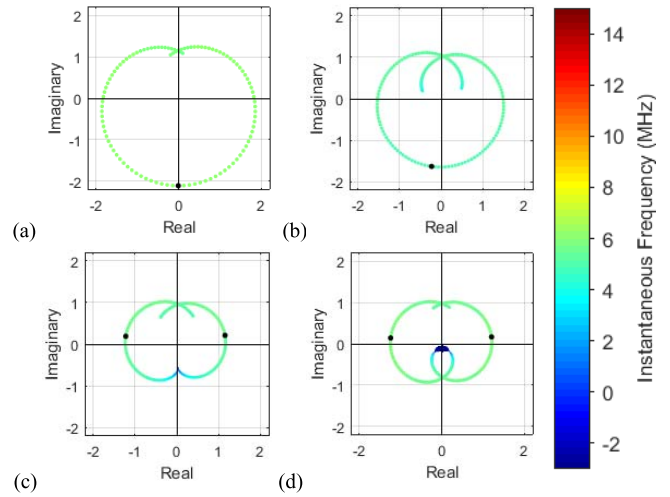

Fig. 7. Modeled analytic signals at four locations along the simulated ply drop shown in Fig. 5, with resin-wedge thicknesses of: (a) 0.05 mm (the maximum amplitude), (b) 0.13 mm, (c) 0.21 mm, and (d) 0.25 mm (end of the dropped ply). Colors of the dots indicate instantaneous frequency using the color scale on the right—note blue dots near origin in (d). Large black dots at local-maxima in instantaneous-amplitude show that the front and back wedge echoes split as it thickens; phases move from $\phi_0 - \pi/2$ for a thin resin layer to $\phi_0 + \pi$ and ϕ_0.

the ply drop, which can be seen in Fig. 5(d) as a drop in instantaneous frequency in these plies. The consequence is that the phase progression in the resin wedge is π radians in a gradually increasing propagation time [Fig. 7(c)–(d)]. This is why there is a minimum in amplitude. A negative instantaneous frequency occurs close to the dropped ply—at location 3 mm and time 1.1 μs in Fig. 5—caused by a second-harmonic loop in the phase response and a minimum in the amplitude response (an antiresonance) [see Fig. 7(d)]. The loop grows as the wedge thickens and the π radians phase progression has to fit a longer time period. Fig. 5(e) shows that the resin layers, and front and back surfaces of the resin wedge, can be tracked well from their characteristic signatures.

D. Out-of-Plane Ply Wrinkling

As out-of-plane wrinkling is accompanied by changes in ply thickness, the result is a change in the instantaneous frequency. Fig. 5(d) demonstrates a frequency increase above the wrinkle in the squashed plies and a decrease where the plies are thicker.

The ability of instantaneous phase to track resin layers and map out-of-plane wrinkles [34] works only in the fundamental-resonance mode (see Fig. 2). If the ply becomes too thick, the second-harmonic mode is entered, in which two cycles of phase are traversed per ply; if the ply becomes too thin, the subharmonic mode is entered. This effect on wrinkle imaging can be seen in Fig. 5(c). Where plies are thinner, above the wrinkle, instantaneous frequency increases but stays in the fundamental resonance mode [Fig. 2(c)]. A negative instantaneous frequency occurs when the ply is thicker but not enough to enter the second-harmonic mode [Fig. 2(e)]. If the second-harmonic mode is entered [Fig. 2(f)], a sudden change from negative to high positive frequencies occurs as the loop crosses the origin, giving zero amplitude and causing a phase singularity [47] where phase is unknown.
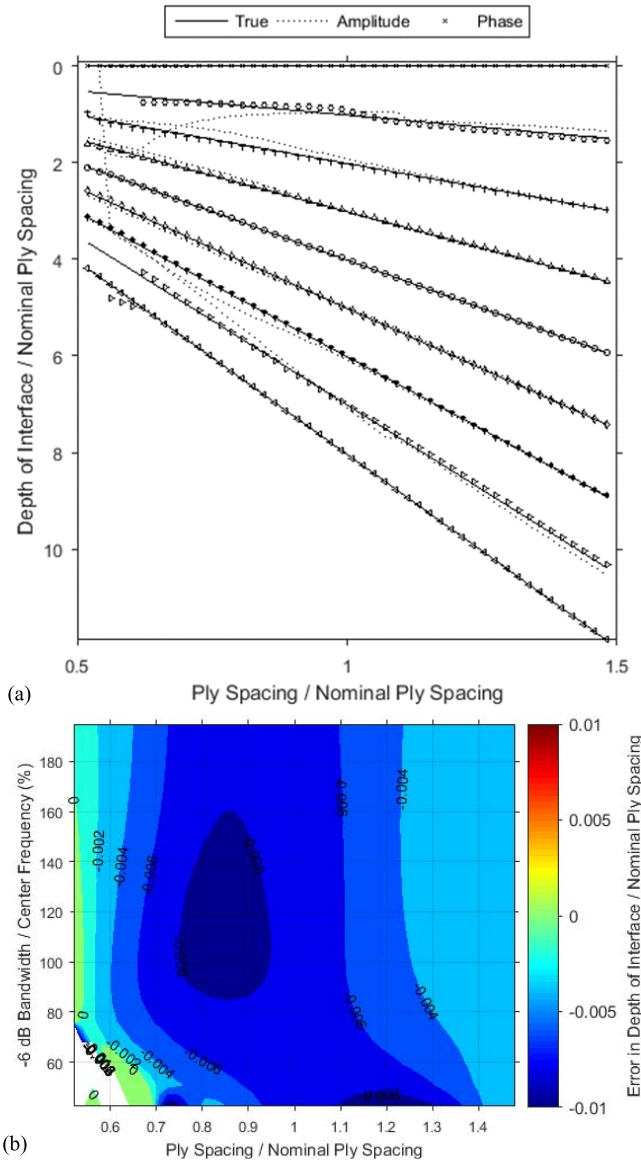
(a)

(b)

Fig. 8.   Ultrasonically measured interface depth compared with true depth in an 8-ply composite, in immersion, for (a) time of phase $\phi_0 - \pi/2$ and time of peak amplitude and (b) error in time of phase of $\phi_0 - \pi/2$ for the middle interface, as a ratio of ply spacing and as a function of bandwidth/center-frequency ratio.

It is important to determine the potential accuracy of ply-interface tracking as a function of ply spacing within a wrinkle for a range of bandwidth/center-frequency ratios. Analytically modeled quantitative information is shown in Fig. 8 for 8 plies in water, where all plies change in thickness whilst the center frequency is kept at the fundamental resonance of the nominal ply spacing. Fig. 8(b) shows that the depth error for the middle resin layer is predicted to be less than ±1% of the nominal ply spacing across the bandwidth range.

E. Summary of Modeling Predictions

The characteristic analytic-signal features of these defects are summarized in Table I and their use to detect and characterize these features is demonstrated in Fig. 5(e) and the following section on experimental applications.
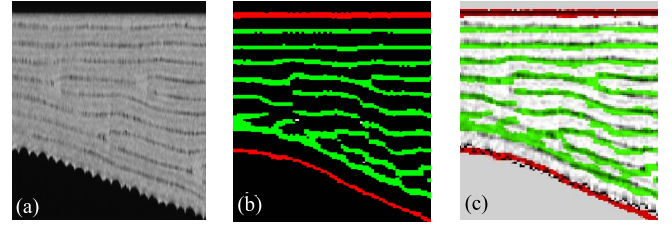

Fig. 9.   Wedge specimen containing ply-drops, made from 0.189-mm plies and incorporating 0.04-mm resin layers. (a) X-ray CT slice. (b) Ultrasound-derived front-surface (red), back-surface (red), and resin-layer (green) locations (c) overlaid on X-ray CT data. The ultrasound scan used a 38-mm spherical-focus 7.5-MHz probe.

V. EXPERIMENTAL APPLICATION

All of the experimental data presented below was acquired using single-element normal-incidence focused probes in immersion with the focal plane at the mid-plane of the sample. A 38-mm focal-length in water has been shown to be a good compromise for probes with center frequencies of 5, 7.5, and 10 MHz. The 7.5-MHz probe reported here was 12.5 mm in diameter so the −6-dB focal spot size in composite was calculated to be 1.2 mm, with a −6-dB focal range (depth of field) of 11 mm in composite. The probe was chosen to have a measured center frequency closest to the fundamental ply-resonance frequency. Olympus Videoscan probes were used because they have a bandwidth approximately equal to the center frequency and this has been shown to be optimal [34]. Pulse-echo full-waveform data was acquired over a 2-D raster scan with a 0.2-mm step size controlled by scanner software from Ultrasonic Sciences Ltd. The data acquisition rate was at least 100 MS/s in all cases.

A. Determining Input-Pulse Phase

The above modeling exercise has demonstrated that phase is effectively "locked" to the interply resin layers and that it is crucial to know the phase, ϕ_0, at the peak instantaneous amplitude of the input pulse for correct location mapping of interfaces. It has also been shown that the front-surface echo can be used to determine the input phase. For the following experimental analysis, the phase was determined at the peak instantaneous amplitude for the mean analytic signal from a large number of waveforms near the middle of the scan.

B. Ply Tracking: Front and Back Surfaces and Resin-Layers

Once the input-pulse phase is known, the analytic-signal formulation allows automatic classification of front surface, back surface, and resin-layer interfaces based on the criteria for instantaneous amplitude, phase and frequency listed in Table I. Fig. 9 shows the result, compared with optical cross sections and X-ray CT, for a wedge specimen with several ply-drop locations. Fig. 10 shows the stages in the process.
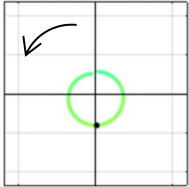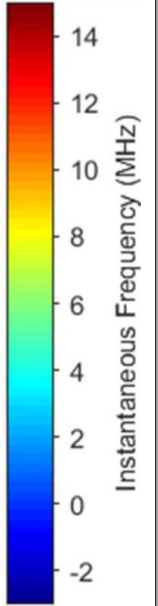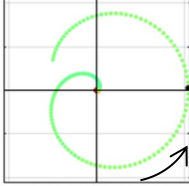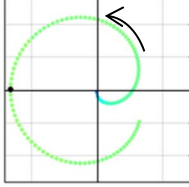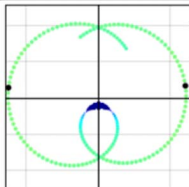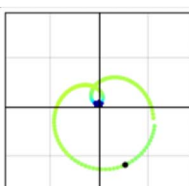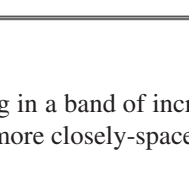
Agreement is very good for all but the interface between the last two plies where the attenuation due to the 0.04-mm resin layers has caused a significant signal reduction.

This wedge specimen was manufactured with a 0.189-mm ply spacing inclusive of 0.04-mm toughened resin layers.

TABLE I

SUMMARY OF THE PREDICTED CHARACTERISTIC ANALYTIC-SIGNAL RESPONSE TO VARIOUS FEATURES IN A COMPOSITE LAMINATE FOR THE SCENARIO WHERE THE CENTER FREQUENCY OF THE INPUT PULSE IS AT THE FUNDAMENTAL PLY RESONANCE FREQUENCY. ϕ_0 IS THE INSTANTANEOUS PHASE AT THE TIME OF THE PEAK AMPLITUDE OF THE INPUT PULSE AND IS SET TO ZERO FOR THE IMAGES IN THE ANALYTIC SIGNAL COLUMN. THE BLACK DOTS IN THOSE IMAGES ARE AT THE PEAKS IN INSTANTANEOUS AMPLITUDE

Analytic-Signal Parameter:	Instantaneous Amplitude	Instantaneous Phase	Instantaneous Frequency	Analytic Signal (for $\varphi_0=0$)	Color scale
Inter-ply resin layers	Small peaks at resin layers.	$\phi_0 - \pi/2$	Higher at resin layer than mid-ply.		
Front surface	Largest peak in the waveform.	ϕ_0	25% lower in the first ply (cyan color in the adjacent analytic-signal plot).		
Back surface	Second largest peak in waveform if no defect.	$\phi_0 - \pi$	25% lower in the last ply (cyan color in adjacent plot).		
Delaminations	Higher than a back-surface signal.	$\phi_0 - \pi$	25% lower in the ply before the delamination.		
Resin-filled ply drops	Higher at front and back of resin wedge.	Resin wedge has phase $\phi_0 - \pi/2 \pm \pi/2$	25% lower in plies above and below the resin wedge. Much lower (negative) at end of the ply that drops.		
Out-of-plane wrinkling	Higher where plies are squashed, lower where plies are expanded. Very low for −ve inst. frequencies.	Resonance mode can change if plies too thick or thin.	Higher where plies are squashed, lower where they are expanded (see next column).		

The fundamental resonance will be approximately 8 MHz and the reflection coefficient of each resin layer will be four or five times larger than for nontoughened resin layers, which will generally have a thickness of 0.005–0.010 mm.

Fig. 11 illustrates characteristic features in the instantaneous frequency at a ply-drop as the resin layer thickens. Where it starts to thicken [red line, Fig. 11(a)], the plies immediately above and below have a lower instantaneous frequency [cyan color in Fig. 11(b)]. The harmonic frequencies continue to reduce until [green line, Fig. 11(a)] a negative-frequency region appears at the end of the dropped ply in Fig. 11(c) because the second-harmonic frequency has become significant in the bandwidth of the probe (the second-harmonic mode). The dropped ply is thinner at its endpoint [yellow line, Fig. 11(a)], resulting in a band of increased instantaneous frequency between two more closely-spaced resin-layer depths as seen in Fig. 11(d).

C. Delaminations

The same process was applied to data from an impact-damaged region in a nontoughened composite with 0.25-mm ply spacing and thin (approximately 0.01-mm thick) resin layers. The classic cone-shaped delamination-damage region can be seen in Fig. 12.

It is important that multiple reflections after a delamination are not misinterpreted as actual deeper delaminations; these have been correctly interpreted by the automated process
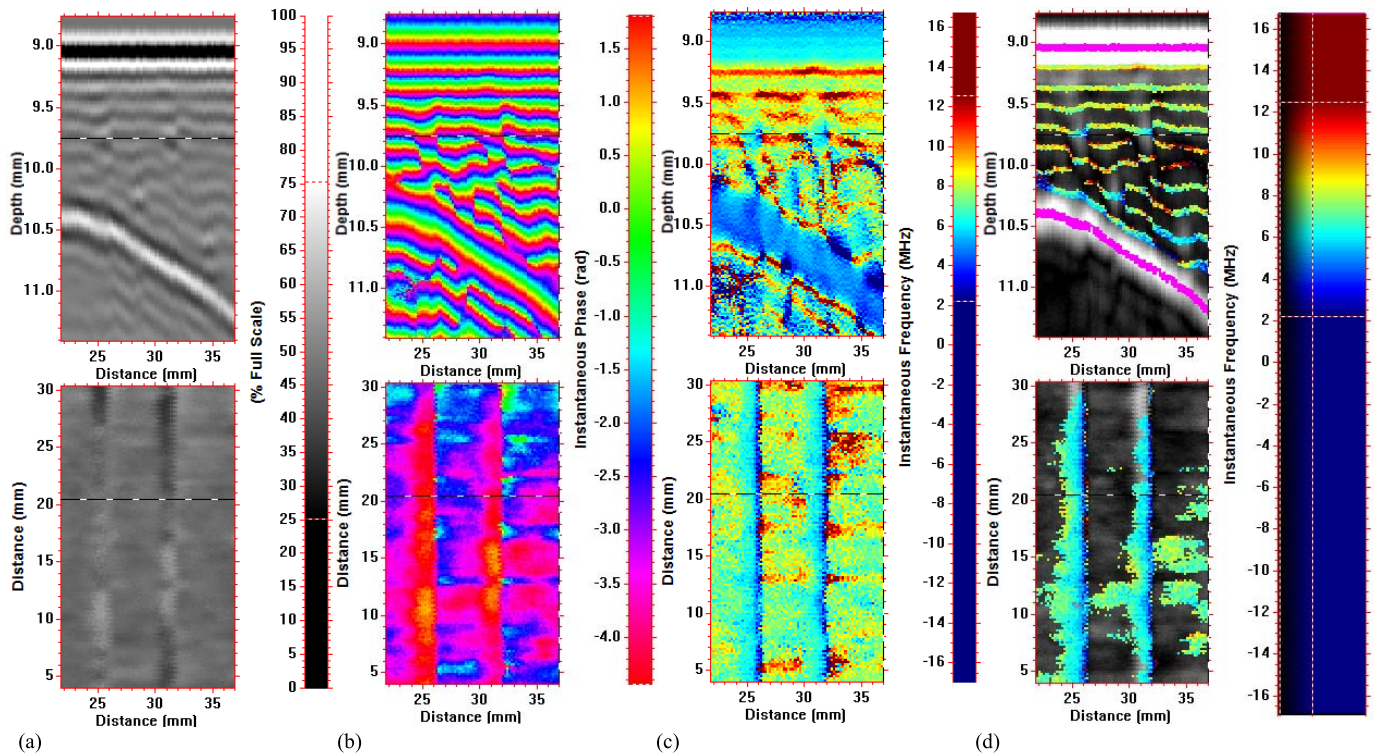
Fig. 10. Ultrasonic B-scan (above) and in-plane (below) slices from a wedge-shaped sample comprising several ply-drops in 0.189-mm-spaced plies with 0.04-mm resin layers. The in-plane slices are from a depth where there are two ply drops. Response parameters shown are (a) RF waveform, (b) instantaneous phase, (c) instantaneous frequency, and (d) instantaneous amplitude with superimposed front and back-surface locations (magenta) and resin layers between plies showing instantaneous frequency (color scale). The ultrasound scan was performed with a 38-mm spherical-focus probe with a 7.5-MHz nominal center frequency.
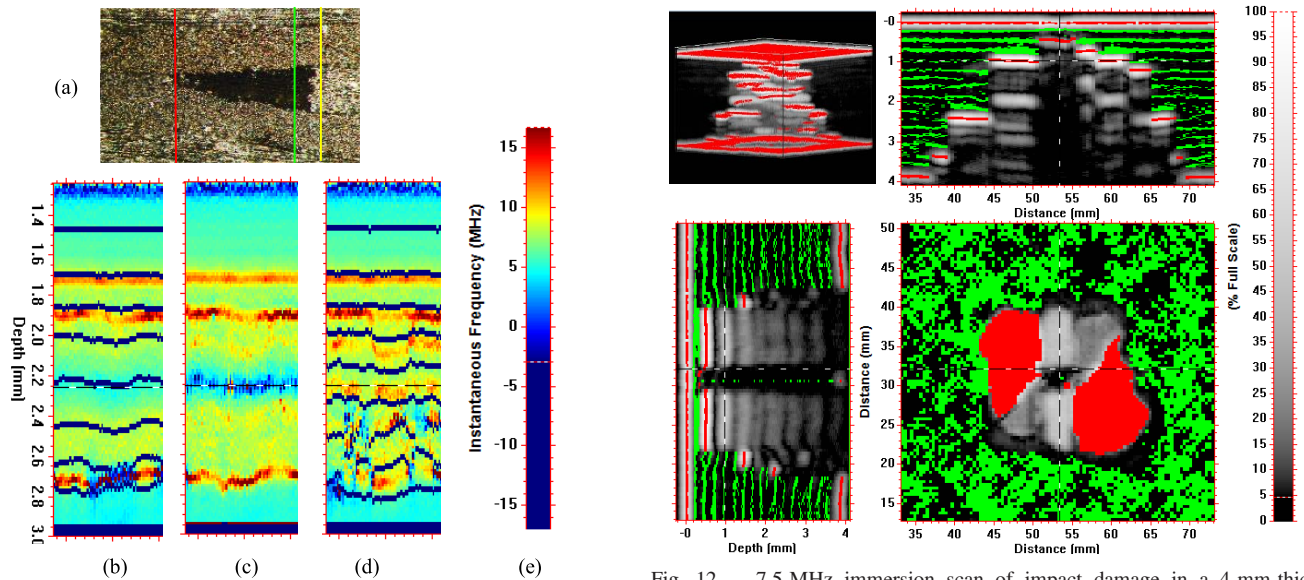

Fig. 11. (a) Micrograph of the resin-filled ply-drop location. (b)–(d) Instantaneous-frequency B-scan cross-sections for the red, green, and yellow-line locations, respectively, in (a). Dark blue lines in (b) and (d) correspond to phase wraps in the instantaneous phase, set at the phase of a resin layer, resulting in a large negative frequency but also marking the location of a resin layer. (e) Color scale for instantaneous frequency.
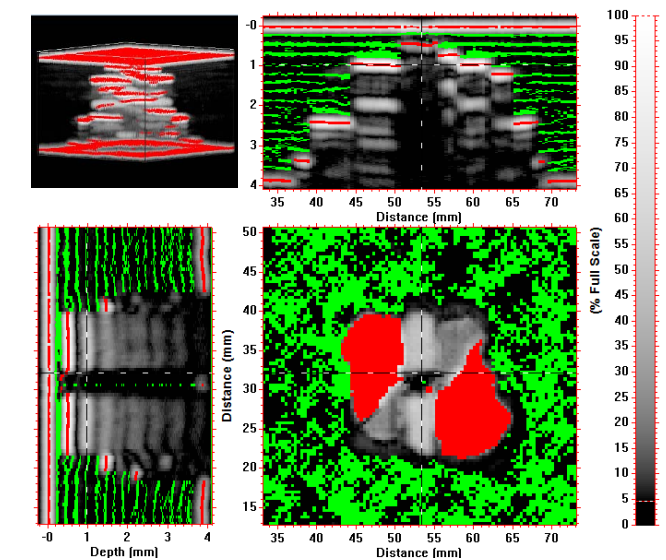

Fig. 12. 7.5-MHz immersion scan of impact damage in a 4-mm-thick composite with 0.25-mm ply spacing. Instantaneous amplitude is plotted in grayscale (right) with overlaid ultrasound-derived coding for front- and back-surfaces (red), delaminations (red), and inter-ply resin layers (green). Bottom-center is an in-plane C-scan slice 1-mm deep, whilst bottom-left and top-center images are B-scan slices at locations shown by black/white dashed lines on the C-scan. Top-left is a pseudo 3-D image with front, back, and delaminations showing red.

which stops looking for interfaces after the first delamination or back-wall echo. Note that the delaminations appear to have been tracked right to their edges in the data.

D. Tape Gaps, Tape Overlaps, and Wrinkles

Gaps or overlaps created at the edges of tapes during the tape lay-up manufacturing process can cause stress
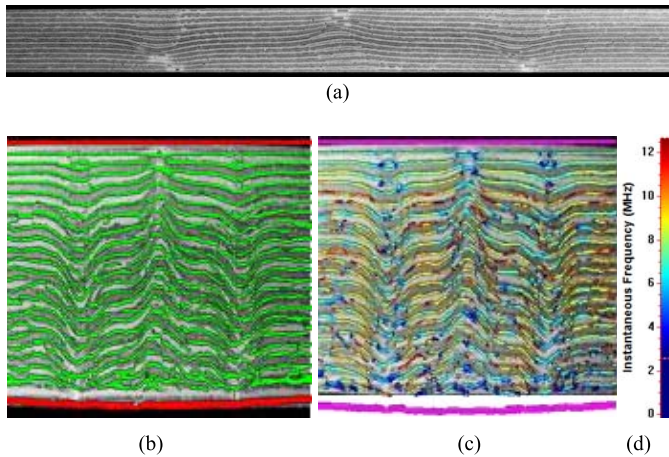
Fig. 13. (a) X-ray CT-scan slice showing tape-gap/overlap cross-ply specimen with the true 1:1 aspect ratio; 0° plies appear darker than 90° plies. (b) and (c) use an aspect ratio to match the ultrasound data. (b) Overlaid red lines for front and back surfaces and green for resin layers. (c) Magenta lines for front and back surfaces and colored lines for instantaneous frequency at resin layers using color scale (d). X-ray parameters were: source voltage: 28 kV, current: 850 μA, exposure time: 2 s, 2400 projections with one shot per projection, Tungsten target, Beryllium window, and detector: GE DXR250.

concentrations and need to be tracked through a laminate. Wrinkles can be created as a side-effect; the 25-ply sample shown in Fig. 13 was manufactured to exhibit all of these features using IMA/M21 (fiber/matrix) material with 0.189-mm ply spacing incorporating approximately 0.02-mm thick resin layers. Tape gaps are in the upper part of the center wrinkle with overlaps in the lower part, whilst this is reversed for the left and right wrinkles. It demonstrates how well the process outlined above can be used to track the resin layers (plotted as colors on an instantaneous frequency scale) and identify tape gaps and overlaps as reductions in instantaneous frequency because they are either thick resin-filled layers or thick double-ply layers. Note that the thin resin layers, which are less reflective, allow adequate transmission through the full 25-ply laminate.

VI. DISCUSSION

Although many composite laminates are uniform over the lateral scale of a focused ultrasonic beam and are therefore suitable for modeling using a 1-D model, certain defect types such as ply drops and any 2-D or 3-D woven composites vary significantly within this scale. Future work by the authors will be focused on the use of 3-D finite-element analysis modeling for woven composites including a comparison with the 1-D model used here [48]. The inversion methods developed in this paper do not rely on the model for their operation but a 3-D model may well help to understand effects of focusing and nonnormal-incidence propagation.

The 1-D model predictions presented in this paper have increased understanding of the ultrasonic response from flat laminates sufficiently to propose new methods to invert the ultrasonic data. These methods have been shown to work well with a few flat samples containing ply drops, tape gaps and overlaps, wrinkles, and delaminations. However, in these

results there is evidence that this is not yet the complete picture. For example, in Fig. 9, the ply tracking appears to become confused beyond about 8 plies in depth in this sample with 0.04-mm resin layers, whereas the tracking is good until about ply 20 in Fig. 13 where the resin layers are only 0.02-mm thick. This is thought to be caused by phononic band gaps, where the resonance frequency is selectively attenuated due to its stronger reflection from thicker plies. This effect is undergoing further investigation; an explanation and further results are published in [49]. The authors are also investigating solutions to this problem in terms of signal processing or detection and correction of the effects in the data.

There are also several outstanding issues to do with the setting of thresholds and other parameters for the gates used for ply tracking shown in Fig. 6. The primary concern here is the ability to distinguish between resin-layer reflections and the back surface or delamination signals but without erroneously classifying a ply-drop as a delamination. The proposed criteria on instantaneous amplitude may be difficult to calculate on a very wide range of materials, numbers of plies, attenuations, and entry/exit media. The drop in instantaneous frequency in the last ply before the back surface or a delamination is a crucial clue here, but this also exists before a ply drop and may be subject to other ply-thickness variations in the structure. Further work is being undertaken to investigate rigorous methods for calculating these thresholds.

Finally, there is evidence in Fig. 13 that there is a limit to the out-of-plane ply angle that can be tracked consistently through the structure. The previous work has suggested a maximum measurable angle of 15° and, below this, an accuracy of $\pm(2° + 17\%)$ [30], but this has yet to be verified for the latest ply-tracking algorithms. Future work will include a new investigation of limitations and measurement uncertainties.

VII. CONCLUSION

The aim of this paper was to develop an automated process for characterizing composite laminates based on characteristic signatures of microstructural features. Use of the analytic-signal formulation of the ultrasonic response has added three metrics to the conventional armory of ultrasonic NDT measurements—instantaneous amplitude, instantaneous phase, and instantaneous frequency. In composite laminates, these metrics have been shown by 1-D analytical modeling to be sensitive to small variations in layer thicknesses, which are characteristic of features and defects that are of great interest to manufacturers, such as ply drops, tape gaps and overlaps, out-of-plane wrinkles, and delaminations. Depending on the ply spacing in the composite, the transducer center frequency and bandwidth can be chosen to optimize the enhanced imaging of these characteristic signatures.

A process has been demonstrated for automatically recognizing, measuring, and mapping the times-of-flight to the front surface, back surface, and all resin-rich layers between plies. This results in a significant enhancement in the 3-D ultrasonic imaging of composite laminates. The maps of these interface locations from experimental data have been qualitatively compared with both optical micrographs and X-ray CT scans for components containing ply drops, delaminations, and wrinkles.

Two different resin-rich interply layer thicknesses were tested experimentally and the automated processing was applied. Agreement with X-ray CT and microsectioning was good for the sample with 0.02 mm resin layers, throughout 25 plies to the back surface. It was also good for the first plies of the sample with thick (0.04 mm) resin layers, but became poorer deeper than approximately 10 plies. This is due to the increased attenuation of the resonance frequency; the reflection coefficient from resin layers increases approximately linearly with resin-layer thickness.

The tracking of interfaces through ply drops, tape gaps, tape overlaps, and wrinkles is a severe test of the process, which has performed well in all of these cases provided the optimum data acquisition parameters for center frequency and bandwidth are used. However, there is still further work to do to unambiguously differentiate delaminations from ply drops because they both show a reduction in instantaneous frequency and an increase in amplitude compared with resin layers.

ACKNOWLEDGMENT

REFERENCES

[1] A. Caiazzo, M. Orlet, H. McShane, L. Strait, and C. Rachau, "The effects of marcel defects on composite structural properties," in *Composite Structures Theory and Practice* (ASTM Special Technical Publication 1383), P. Grant and C. Q. Rousseau, Eds. West Conshohocken, PA, USA: ASTM, 2000, pp. 158–187.

[2] W. J. Cantwell and J. Morton, "The significance of damage and defects and their detection in composite materials: A review," *J. Strain Anal. Eng. Des.*, vol. 27, no. 1, pp. 29–42, 1992.

[3] R. A. Smith, Ed., *Report From the Workshop on NDT and SHM Requirements for Aerospace Composites*. Northampton, U.K.: British Institute Non-Destructive Testing, 2016, doi: 10.1784/book.2016.001.

[4] Y. Nikishov, A. Makeev, G. Seon, E. Bostaph, and E. Armanios, "Challenges and perspectives for nondestructive inspection and structural diagnostics of composites," in *Proc. 40th Eur. Rotorcraft Forum*, Southampton, U.K., 2014, pp. 1–12.

[5] J. Kastner, B. Plank, A. Reh, D. Salaberger, and C. Heinzl, "Advanced X-ray tomographic methods for quantitative characterisation of carbon fibre reinforced polymers," in *Proc. 4th Int. Symp. NDT Aerosp.*, 2012, pp. 1–9.

[6] J. Weissenböck *et al.*, "FiberScout: An interactive tool for exploring and analyzing fiber reinforced polymers," in *Proc. IEEE Pacific Vis. Symp.*, Mar. 2014, pp. 153–160.

[7] A. Bhattacharya, C. Heinzl, A. Amirkhanov, J. Kastner, and R. Wenger, "MetaTracts—A method for robust extraction and visualization of carbon fiber bundles in fiber reinforced composites," in *Proc. IEEE Pacific Vis. Symp. (PacificVis)*, Apr. 2015, pp. 191–198.

[8] R. F. Anastasi, "Investigation of fiber waviness in a thick glass composite beam using THz NDE," *Proc. SPIE 6934*, p. 69340K, Apr. 2008.

[9] C. Jördens *et al.*, "Terahertz spectroscopy to study the orientation of glass fibres in reinforced plastics," *Compos. Sci. Technol.*, vol. 70, no. 3, pp. 472–477, Mar. 2010.

[10] K. Mizukami, Y. Mizutani, K. Kimura, A. Sato, A. Todoroki, and Y. Suzuki, "Detection of in-plane fiber waviness in cross-ply CFRP laminates using layer selectable eddy current method," *Compos. A, Appl. Sci. Manuf.*, vol. 82, pp. 108–118, Mar. 2016.

[11] H. Heuer *et al.*, "Review on quality assurance along the CFRP value chain—Non-destructive testing of fabrics, preforms and CFRP by HF radio wave techniques," *Compos. B, Eng.*, vol. 77, pp. 494–501, Aug. 2015.

[12] C. A. C. Leckey and P. D. Juarez, "Simulation of guided wave interaction with in-plane fiber waviness," in *Proc. AIP Conf.*, 2017, p. 020023.

[13] R. F. Elhajjar, S. S. Shams, G. J. Kemeny, and G. Stuessy, "A hybrid numerical and imaging approach for characterizing defects in composite structures," *Compos. A, Appl. Sci. Manuf.*, vol. 81, pp. 98–104, Feb. 2016.

[14] M. P. F. Sutcliffe, S. L. Lemanski, and A. E. Scott, "Measurement of fibre waviness in industrial composite components," *Compos. Sci. Technol.*, vol. 72, no. 16, pp. 2016–2023, Nov. 2012.

[15] K. K. Kratmann, M. P. F. Sutcliffe, L. T. Lilleheden, R. Pyrz, and O. T. Thomsen, "A novel image analysis procedure for measuring fibre misalignment in unidirectional fibre composites," *Compos. Sci. Technol.*, vol. 69, no. 2, pp. 228–238, Feb. 2009.

[16] S. W. Yurgartis, "Measurement of small angle fiber misalignments in continuous fiber composites," *Compos. Sci. Technol.*, vol. 30, no. 4, pp. 279–293, 1987.

[17] A. Clarke, G. Archenhold, and N. Davidson, "A novel technique for determining the 3D spatial distribution of glass fibres in polymer composites," *Compos. Sci. Technol.*, vol. 55, no. 1, pp. 75–91, 1995.

[18] A. Sandhu, T. J. Dodwell, and R. Butler, "An automated processing algorithm to determine wrinkle characteristics from B-scans," in *Proc. 17th Eur. Conf. Compos. Mater.*, 2016, pp. 1–8.

[19] M. Kersemans *et al.*, "The ultrasonic polar scan for composite characterization and damage assessment: Past, present and future," *Appl. Sci.*, vol. 6, no. 2, p. 58, 2016.

[20] J.-P. Zardan, C. Gueudré, and G. Corneloup, "Study of induced ultrasonic deviation for the detection and identification of ply waviness in carbon fibre reinforced polymer," *NDT&E Int.*, vol. 56, pp. 1–9, Jun. 2013.

[21] S. K. Chakrapani, V. Dayal, and D. Barnard, "Detection and characterization of waviness in unidirectional GFRP using Rayleigh wave air coupled ultrasonic testing (RAC-UT)," *Res. Nondestruct. Eval.*, vol. 24, no. 4, pp. 191–201, 2013.

[22] R. A. Smith, "Use of 3D ultrasound data sets to map the localised properties of fibre-reinforced composites," Ph.D. dissertation, Dept. Elect. Eng., Univ. Nottingham, Nottingham, U.K., 2010.

[23] M. J. Mienczakowski, "Advanced ultrasonic NDE of composite airframe components: Physics, modelling and technology," Ph.D. dissertation, Dept. Elect. Eng., Univ. Nottingham, Nottingham, U.K., 2010.

[24] Y. Humeida, V. J. Pinfield, and R. E. Challis, "Modelling ultrasonic array signals in multilayer anisotropic materials using the angular spectrum decomposition of plane wave responses," *J. Phys., Conf. Ser.*, vol. 457, no. 1, p. 012005, 2013.

[25] Y. Humeida, V. J. Pinfield, R. E. Challis, P. D. Wilcox, and C. Li, "Simulation of ultrasonic array imaging of composite materials with defects," *IEEE Trans. Ultrason., Ferroelect., Freq. Control*, vol. 60, no. 9, pp. 1935–1948, Sep. 2013.

[26] R. A. Smith and B. Clarke, "Ultrasonic C-scan determination of ply stacking sequence in carbon-fiber composites," *Insight-J. Brit. Inst. NDT*, vol. 36, no. 10, pp. 741–747, 1994.

[27] D. Hsu, D. Fei, and Z. Liu, "Ultrasonically mapping the ply layup of composite laminates," *Mater. Eval.*, vol. 60, no. 9, pp. 1099–1106, 2002.

[28] R. A. Smith, L. J. Nelson, M. J. Mienczakowski, and R. E. Challis, "Automated analysis and advanced defect characterisation from ultrasonic scans of composites," *Insight-J. Brit. Inst. NDT*, vol. 51, no. 2, pp. 82–87, Feb. 2009.

[29] L. J. Nelson and R. A. Smith, "Three-dimensional fibre-orientation characterisation in monolithic carbon-fibre composites," in *Proc. Eur. Conf. NDT*, Prague, Czech Republic, 2014, pp. 1–12.

[30] R. A. Smith, L. J. Nelson, N. Xie, C. Fraij, and S. R. Hallett, "Progress in 3D characterisation and modelling of monolithic carbon-fibre composites," *Insight-J. Brit. Inst. NDT*, vol. 57, no. 3, pp. 131–139, 2015.

[31] D. Pain and B. W. Drinkwater, "Detection of fibre waviness using ultrasonic array scattering data," *J. Nondestruct. Eval.*, vol. 32, no. 3, pp. 215–227, 2013.

[32] D. Pain and B. W. Drinkwater, "Detection of fiber waviness in composites using ultrasonic arrays," in *Proc. ICEM16*, 2013, pp. 1–2.

[33] C. Li, D. Pain, P. D. Wilcox, and B. W. Drinkwater, "Imaging composite material using ultrasonic arrays," *NDT&E Int.*, vol. 53, pp. 8–17, Jan. 2013.

[34] R. A. Smith, L. J. Nelson, M. J. Mienczakowski, and P. D. Wilcox, "Ultrasonic tracking of ply drops in composite laminates," in *Proc. AIP Conf.*, vol. 1706. 2016, p. 050006, doi: 10.1063/1.4940505.

[35] Z. Hashin, "On elastic behaviour of fibre reinforced materials of arbitrary transverse phase geometry," *J. Mech. Phys. Solids*, vol. 13, no. 3, pp. 119–134, Jun. 1965.

[36] Z. Hashin, "Analysis of properties of fiber composites with anisotropic constituents," *J. Appl. Mech.*, vol. 46, no. 3, pp. 543–550, Sep. 1979.

[37] D. Gabor, "Theory of communication. Part 1: The analysis of information," *J. Inst. Elect. Eng.*, vol. 93, no. 26, pp. 429–457, 1946.

[38] P. M. Gammell, "Improved ultrasonic detection using the analytic signal magnitude," *Ultrasonics*, vol. 19, no. 2, pp. 73–76, 1981.

[39] R. C. Heyser, "Determination of loudspeakier signal arrival times: Part III," *J. Audio Eng. Softw.*, vol. 19, no. 11, pp. 902–905, 1971.

[40] S. C. Kak, "The discrete Hilbert transform," *Proc. IEEE*, vol. 58, no. 4, pp. 585–586, Apr. 1970.

[41] B. Boashash, "Estimating and interpreting the instantaneous frequency of a signal. I. Fundamentals," *Proc. IEEE*, vol. 80, no. 4, pp. 520–538, Apr. 1992.

[42] Z. W. Bell, "Use of the analytic signal in ultrasonic imaging," in *Review of Progress in Quantitative Nondestructive Evaluation*, vol. 4A, D. O. Thompson and D. E. Chimenti, Eds. New York, NY, USA: Plenum Press, 1985, pp. 327–332.

[43] J. D. Foley, *Computer Graphics: Principles and Practice*, 2nd ed. Redwood City, CA, USA: Addison-Wesley, 1995.

[44] P. R. Woodward, "Interactive scientific visualization of fluid flow," *Computer*, vol. 26, no. 10, pp. 13–25, Oct. 1993.

[45] S. Giannis, V. Matěják, and R. Freemantle, "Maximising the benefit of non-destructive Inspection data to evaluate the damage Tolerance performance of composites," in *Proc. SAMPE Tech. Conf.*, Wichita, KS, USA, 2013, pp. 1–17.

[46] R. Freemantle, S. Giannis, and V. Matěják, "Phased array data manipulation for damage tolerance assessment of composites using finite element analysis," in *Proc. 11th Eur. Conf. NDT (ECNDT)*, Prague, Czech Republic, 2014, pp. 1–10.

[47] J. F. Nye and M. V. Berry, "Dislocations in wave trains," *Proc. Roy. Soc.*, vol. 336, no. 1605, pp. 165–190, Jan. 1974, doi: 10.1098/rspa.1974.0012.

[48] R. B. Tayong, M. J. Mienczakowski, and R. A. Smith, "3D ultrasound characterization of woven composites," in *Proc. AIP Conf. Rev. Prog. Quantitative NDE*, 2018.

[49] R. A. Smith, L. J. Nelson, and M. J. Mienczakowski, "Phononic band gaps and phase singularities in the ultrasonic response from toughened composites," in *Proc. AIP Conf. Rev. Prog. Quant. NDE*, 2018.

Luke J. Nelson studied materials science and engineering at the University of Bath, Bath, U.K., where he also received the Ph.D. degree in the field of piezoelectric materials in 2004.

He spent seven years at QinetiQ Ltd, Farnborough, U.K. working in the field of non-destructive testing, and currently is a Senior Research Associate with the Ultrasonics and NDT Research Group, University of Bristol, Bristol, U.K.

Martin J. Mienczakowski studied electronics and communications engineering and received the Ph.D. degree in the ultrasonic inspection of composites from the University of Nottingham, Nottingham, U.K.

In 2008, he joined Rolls-Royce Nuclear, Derby, U.K., where he was involved in the implementation of full-matrix capture in nuclear plant components. From 2014 to 2016, he was a Senior Research Associate with the Ultrasonics and NDT Research Group, University of Bristol, Bristol, U.K., he has been a senior-school Physics Teacher since July 2017. His research interests include the inspection of composites, the optimization of phased-array inspection, and the use of full-matrix capture in the nuclear industry.

Dr. Mienczakowski was the first Chair of the ICNDT Special-Interest Group on full matrix capture and was the Chair of the Aerospace Group, British Institute of Nondestructive Testing.

Robert A. Smith received the B.A. degree in physics from the University of Cambridge, Cambridge, U.K., the M.Sc. degree in applied acoustics from Kings College, London, U.K., and the Ph.D. degree in the ultrasonic 3-D characterization of fiber-reinforced composites from the University of Nottingham, Nottingham, U.K.

He is currently a Professor of NDT and high value manufacturing with the University of Bristol, Bristol, U.K. He spent six years at the National Physical Laboratory, Teddington, U.K. and then joined the Nondestructive Evaluation (NDE) Group, Royal Aerospace Establishment (RAE), Farnborough, U.K., in 1989. After several years as Fellow in NDE, at the Defence Evaluation and Research Agency, Farnborough, U.K. and QinetiQ Ltd., Farnborough, he became a QinetiQ Senior Fellow in 2011. He moved to the University of Bristol in April 2013 to accept a personal chair and commence a 5-year Engineering and Physical Sciences Research Council Fellowship in Manufacturing entitled "NDT for High Value Manufacturing of Composites." He has authored more than 110 publications.

Prof. Smith was a recipient of the John Grimwade Medal five times and the Roy Sharpe Prize, awarded by the British Institute of NDT in 1996. He was the President from 2015 to 2016, and is a Fellow of the British Institute of NDT. He is also a Fellow of the Institute of Physics, a Chartered Physicist, and a Chartered Engineer.

Paul D. Wilcox was born in Nottingham, U.K., in 1971. He received the M.Eng. degree in engineering science from the University of Oxford, Oxford, U.K., in 1994, and the Ph.D. degree from Imperial College, London, U.K., in 1998.

Since 2002, he has been with the Department of Mechanical Engineering at the University of Bristol, Bristol, U.K., where his current title is Professor of Dynamics. He held an EPSRC Advanced Research Fellowship in Quantitative Structural Health Monitoring from 2007 to 2012 and is currently Head of the Mechanical Engineering Department. His research interests include array transducers, embedded sensors, ultrasonic particle manipulation, long-range guided wave inspection, structural health monitoring, elastodynamic scattering, and signal processing.